STRUCTURAL CHEMISTRY

ISSN 2053-2296

Diffuse scattering in silver hypodiphosphate, $Ag_4(P_2O_6)$, probed by 3D ED

Vasyl Kinzhybalo,[a]* Jakub Wojciechowski,[b] Dorota A. Kowalska,[a] Vladyslav Maliuzhenko[c] and Katarzyna A. Ślepokura[c]

[a]Institute of Low Temperature and Structure Research, Polish Academy of Sciences, 2 Okólna, Wrocław, 50-422, Poland, [b]Rigaku Europe SE, Hugenottenallee 167, Neu Isenburg, D-63263, Germany, and [c]Faculty of Chemistry, University of Wrocław, 14 F. Joliot-Curie, Wrocław, 50-383, Poland. *Correspondence e-mail: kinzhybalo@gmail.com

Received 6 August 2025
Accepted 12 May 2026

Edited by E. Reinheimer, Rigaku Americas Corporation, USA

This article is part of the collection *Advances in electron diffraction for structural characterization*.

Keywords: powder diffraction; electron diffraction; silver hypodiphosphate; diffuse scattering; real structure; geometric frustration.

CCDC references: 2553762; 2553761; 2553760

Supporting information: this article has supporting information at journals.iucr.org/c

The crystal structure of silver hypodiphosphate, $Ag_4(P_2O_6)$, was determined using 3D ED. The average structure is hexagonal, described in the space group $P6_3/mcm$, and is isomorphous with the average structure of known $Li_4(P_2S_6)$. The silver cations form hexagonal atomic ring layers and the hypodiphosphate anions occupy channels that centre every hexagonal ring, with the P—P bond oriented along the unique c axis. The hypodiphosphate $P_2O_6^{4-}$ anions are disordered, with the P atoms occupying two positions having 50% occupancy each and with O atoms common for both positions of the anion. The O atoms form an octahedral coordination environment for the silver cations. The hypodiphosphate anions are stacked into columns along the unique axis direction. Neighbouring hypodiphosphate columns may have P—P bonds on the same (ferro-type) or on different (antiferro-type) levels. This correlated disorder manifests itself in diffuse scattering observed on hkl layers with uneven l values. Simulations based on an Ising-type model with geometric frustration align well with the experimental data, providing insight into the short-range antiferro-like arrangement of disordered hypodiphosphate anions.

1. Introduction

Nowadays, the crystal structure determination of new materials has become routine for even sub-micron monocrystalline samples, largely thanks to the state-of-the-art electron diffractometers (Ito *et al.*, 2021). Knowledge of the structure is important in terms of understanding the 'composition–structure–properties' relationship, which is vital in the design of new materials with desired properties. However, sometimes the real structure differs from the average one, *i.e.* that determined by an analysis of Bragg diffraction. These differences may prove to be important and have a considerable effect on the properties of the material (Schmidt *et al.*, 2023). One of the well-known examples of such structures are the triangular lattices with antiferro-type interactions between closest neighbours (Keen & Goodwin, 2015). The inability to completely satisfy the antiferro arrangement in the triangular lattice leads to disordered structures with eventual correlations in the disorder.

Since the first report on hypodiphosphoric acid, $H_4P_2O_6$ (Fig. 1), in 1877 by Theodor Salzer until nowadays, knowledge relating to the crystal structures of simple inorganic hypodiphosphates remains quite limited, especially in comparison with other common inorganic phosphates (Kinzhybalo *et al.*, 2021). However, in recent years, there has been an increase in the number of reports of inorganic hypodiphosphates: lithium, sodium and ammonium salts have been systematically investigated for their crystal structures and properties, including

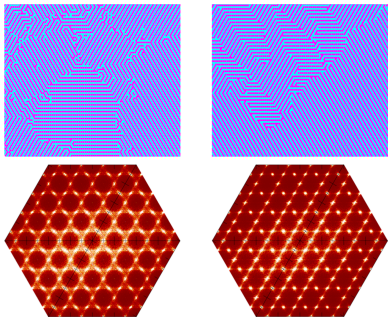

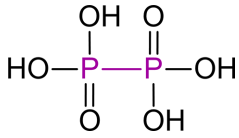

Figure 1
The structural formula of hypodiphosphoric acid.

ionic conductivity in $Na_4(P_2O_6)$ (Szafranowska *et al.*, 2012; Kinzhybalo *et al.*, 2024; Ślepokura *et al.*, 2025; Otręba *et al.*, 2026), ferroelectricity in $(NH_4)_2(H_2P_2O_6)$ (Szklarz *et al.*, 2011), electron-density distribution in $Li_4(P_2O_6)\cdot 6H_2O$ and bis(guanidinium) disodium heptahydrate, $(CH_6N_3)_2Na_2(P_2O_6)\cdot 7H_2O$ (Kinzhybalo *et al.*, 2013; Starynowicz *et al.*, 2025), and thermal stability and spectroscopic properties of many inorganic salts have been reported (Gjikaj *et al.*, 2012; Wu *et al.*, 2012; Gjikaj & Wu, 2014; Gjikaj *et al.*, 2014; Wu *et al.*, 2015; Haase & Gjikaj, 2017; Haase & Gjikaj, 2018).

The first report on the synthesis of $Ag_4(P_2O_6)$ (using phosphorus and a warm acidified solution of silver nitrate) dates back to 1883 (Philipp, 1883). It was also obtained by Joly in 1885 (Joly, 1885) and Salzer in 1886 (Salzer, 1877; Salzer, 1886) in double decomposition reactions. Silver hypodiphosphate was used to obtain organic esters of hypodiphosphoric acid (Sänger, 1886). It was also utilized in a quantitative determination of hypodiphosphate anions in the presence of phosphate and phosphite (Wolf & Jung, 1931). Solid-state ^{31}P NMR spectroscopy was reported for $Ag_4(P_2O_6)$ (Grimmer *et al.*, 1978). Its diffraction pattern along with the unit-cell parameters and space group were deposited in the International Centre for Diffraction Data (Kabekkodu & Blanton, 2024; Kabekkodu *et al.*, 2024) as PDF deposition number 00-047-0901 by H. Worzala in 1996, but a corresponding crystal structure has never been published in the literature. According to the deposited data, $Ag_4(P_2O_6)$ crystallizes in the space group $P6_3/mcm$ and is isostructural with the $Li_4(P_2S_6)$ average structure (Mercier *et al.*, 1982). Both are characterized by disorder of the hypodiphosphate anions within the ordered framework of metal cation positions. The structure of $Li_4(P_2S_6)$ is still under debate in the literature, as there are several reports on its proper space-group determination. The models solved in the space groups $P\bar{3}1m$, *Pnnm* and *Pnma* were considered by Hood *et al.* (2016), but none was given a preference. Dietrich *et al.* (2016) used synchrotron PXRD and PDF analysis and favoured the model in the space group $P\bar{3}1m$. Refinement using NMR crystallography was reported in the space group *P*321 (Neuberger *et al.*, 2018). The same noncentrosymmetric model was reported by Oxley *et al.* (2023) and confirmed by second and third harmonic generation measurements. Yahia *et al.* (2023) reported the twinned single-crystal structure solution in the space group $P\bar{3}m1$. The related selenium-containing material, $Li_4(P_2Se_6)$, turned out to crystallize as a similar, but not isomorphous, form to the thio-analogue crystal form (Neuberger *et al.*, 2025). The other related substance – effective sodium ionic conductor, sodium hexathiohypodiphosphate, $Na_4(P_2S_6)$ – is known to exist in three polymorphic modifications, but none of them is isomorphous with $Li_4(P_2S_6)$ (Scholz *et al.*, 2021; Scholz *et al.*, 2022). Similarly, the recently reported new ionic conductor $Na_4(P_2O_6)$ crystallizes in its own structure type, different from the above-mentioned substances (Kinzhybalo *et al.*, 2024). Knowledge of the proper crystal structure is crucial in understanding lithium and sodium ion conductivity mechanisms in these materials (Li *et al.*, 2020; Stamminger *et al.*, 2020; Hogrefe *et al.*, 2025).

Considering the isomorphism of $Li_4(P_2S_6)$ and $Ag_4(P_2O_6)$, and the disorder of the anions in both compounds, it was interesting to perform detailed structural studies of the latter salt and record subtle diffraction effects that would allow the determination of its real crystal structure. Due to the limited solubility of silver hypodiphosphate in water, crystallization from aqueous solution gives a nanocrystalline material. Therefore, electron diffraction was employed to determine the crystal structure of $Ag_4(P_2O_6)$, and to record and study the diffuse scattering that originates from the correlations in disorder of the hypodiphosphate anions.

2. Experimental

The obtained material was characterized using scanning electron microscopy (SEM) with energy dispersive X-ray analysis (EDX), three-dimensional electron diffraction (3D ED), powder X-ray diffraction (PXRD), variable-temperature PXRD (VT-PXRD), thermogravimetry–differential scanning calorimetry (TG–DSC) and variable-temperature optical microscopy.

2.1. Preparation

Hypodiphosphoric acid was obtained by red phosphorus oxidation with H_2O_2 and was further neutralized with NaOH to give crystalline $Na_2(H_2P_2O_6)\cdot 6H_2O$ (Yoza & Ohashi, 1965). The title material was obtained by mixing stoichiometric amounts of $Na_2(H_2P_2O_6)\cdot 6H_2O$ (314 mg, 1.00 mmol) and Ag_2SO_4 (624 mg, 2.00 mmol) dissolved in a minimum amount of distilled water. A white precipitate was formed immediately and gradually darkened over time. The precipitate was filtered off, washed with water and dried, yielding a slightly brownish grey powder.

2.2. Methods

2.2.1. Scanning electron microscopy (SEM) with energy dispersive X-ray analysis (EDX)

The electron microscopy imaging of the sample and its elemental composition were studied using the field-emission scanning electron microscope (FE-SEM) FEI Nova NanoSEM 230, along with an energy dispersive X-ray spectrometer (EDAX Genesis XM4).

2.2.2. Thermogravimetry–differential scanning calorimetry (TG–DSC)

TG–DSC analysis of $Ag_4(P_2O_6)$ (12.57 mg) was performed using a Mettler–Toledo TGA/DSC 3+ instrument in the temperature range 303–1073 K with a ramp rate of 10 K min^{-1}.

The scans were performed in flowing nitrogen (flow rate: 3 dm^3 h^{-1}).

2.2.3. Variable-temperature microscopy

Optical observations were carried out on an Olympus BX53 microscope equipped with a Linkam THMS 600 temperature adapter and a CCD XC50 video camera in the temperature range 293–593 K.

2.2.4. Room-temperature and variable-temperature PXRD

The PXRD data for the Rietveld refinement of $Ag_4(P_2O_6)$ were collected at room temperature on a PANalytical X'Pert Pro θ–2θ powder X-ray diffractometer using β-filtered Cu $K\alpha$ radiation in the 2θ range 15–132°, with a scan step of 0.007°. The background was fitted as a 9-parameter polynomial. Peak shape was approximated with a pseudo-Voigt profile function. A scale factor and specimen displacement were refined. The coordinates (with special position restrains) and anisotropic B factors of all the atoms were refined.

Variable-temperature powder X-ray diffraction (VT-PXRD) analysis of the $Ag_4(P_2O_6)$ sample was performed on the same PANalytical X'Pert Pro diffractometer with an Anton Paar HTK 1200N high-temperature chamber. Data were collected in the 2θ range 10–90° every 50 K in the temperature range 300–850 K. All Rietveld refinements were performed using the *HighScore Plus* program (Degen *et al.*, 2014).

2.2.5. Electron diffraction data collection and refinement

The crystal structure was determined by 3D electron diffraction (3D ED) from a *ca* 400 nm single crystal rotated about one axis by 120° (scan width 0.5°, 240 images) and with a 0.5 s/° exposure time. The data were collected at ambient temperature *in vacuo* using a Rigaku Synergy-ED diffractometer equipped with a Rigaku HyPix-ED detector optimized for electron detection and an LaB_6 electron source at 200 kV (λ = 0.0251 Å) (Ito *et al.*, 2021). Data collections, cell refinements, data reductions and analysis were carried out with *CrysAlis PRO* (Rigaku OD, 2022). Due to the high symmetry of the phase, this single scan resulted in 87% completeness (up to 0.6 Å resolution). The structure was solved with *SHELXT* (Sheldrick, 2015). Both kinematical and dynamical refinements were carried out in *OLEX2* (Dolomanov *et al.*, 2009). Anisotropic displacement parameters for all atoms were refined. The electron scattering atomic factors of UCLA were used (Saha *et al.*, 2022). The average crystal structure model from dynamical 3D ED refinement (hexagonal crystal system, space group $P6_3/mcm$) was finally refined *versus* powder diffraction data.

Details of the kinematical and dynamical crystal structure refinements, along with the PXRD Rietveld fit details, are given in Table 1.

The *DIAMOND* program (Brandenburg, 2022) was used to produce the figures. All diffraction patterns in this study were calculated using the program *DIFFUSE* (Proffen & Neder, 1997).

Table 1
Crystallographic data for kinematical and dynamical refinement *versus* ED data, and Rietveld refinement *versus* PXRD data.

Chemical formula	$Ag_4P_2O_6$
M_r (g mol^{-1})	589.42
Crystal system, space group	Hexagonal, $P6_3/mcm$
Temperature (K)	293
a, c (Å)	5.39128 (7), 6.30229 (9)
V (Å^3)	158.640 (5)
Z	1
3D ED refinement	
Radiation type	200 kV electron beam (λ = 0.0251 Å)
θ range (°)	0.153–1.162
R_1 (kinematical/dynamical refinement)	0.116/0.122
wR_2 (kinematical/dynamical refinement)	0.400/0.281
Rietveld refinement	
Radiation type	Cu $K\alpha$ (λ = 1.5418 Å)
R (Bragg)	0.032
R (expected)	0.012
R (profile)	0.034
R (weighted profile)	0.051

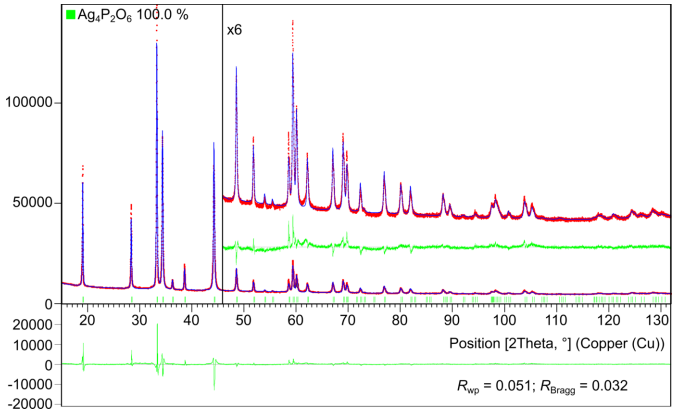

Figure 2
Rietveld fit of the PXRD data of the bulk sample using the average structure model from the dynamical refinement of the 3D ED data (room temperature, 2θ range 15–132°).

3. Results and discussion

3.1. Sample characterization

As mentioned above, the diffraction pattern, unit-cell parameters and space group, but not the atomic coordinates, for $Ag_4(P_2O_6)$ were revealed in the database (ICDD, PDF deposition number 00-047-0901) (Kabekkodu & Blanton, 2024; Kabekkodu *et al.*, 2024). We determined the crystal structure of the title compound by 3D ED and used the atomic model for the Rietveld refinement against the powder diffraction data (Fig. 2 and Fig. S1 in the supporting information). PXRD showed no signs of crystalline silver or any other impurities.

SEM images with EDX analysis of the sample of the title compound showed hexagonal plate- and rod-shaped crystals,

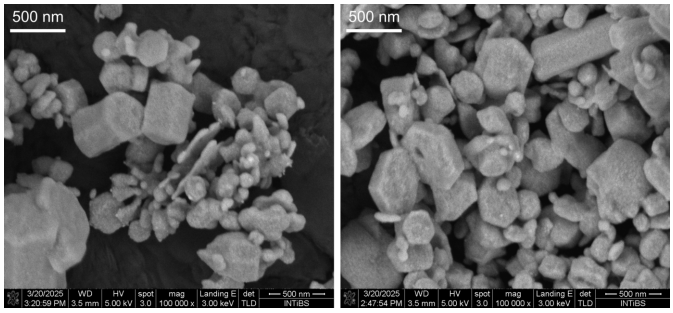

Figure 3
Representative electron microscopy images of the bulk sample (*cf* Figs. S2 and S3 in the supporting information).

and confirmed the $Ag_4(P_2O_6)$ composition (Fig. 3 and Figs. S2 and S3 in the supporting information).

3.2. Stability

Silver hypodiphosphate undergoes partial decomposition within a few minutes after its precipitation, and the snowy white material turns greyish. Despite that, powder diffraction of several months old samples does not reveal any reflections from additional crystalline phases. Thermogravimetric analysis combined with differential scanning calorimetry (TG–DSC, sample mass m = 12.57 mg, ramp rate = 10 K min^{-1}) does not reveal any considerable mass loss ($\Delta m = 6.7 \times 10^{-2}$ mg, 0.5%) in the whole temperature range from 303 to 1073 K. However, the DSC curve shows several energetic processes in this range: three exothermic, around 500, 620 and 1020 K, and one endothermic, around 750 K (Fig. S4 in the supporting information). Variable-temperature optical microscopy performed in the temperature range 293–593 K (40 K min^{-1}), along with variable-temperature powder diffraction (VT-PXRD), were used for a better description and documentation of the processes. As seen in Fig. 4 (and Fig. S5 in the supporting information), the powder melts between 533 and 543 K, and transforms into semi-transparent glassy drops.

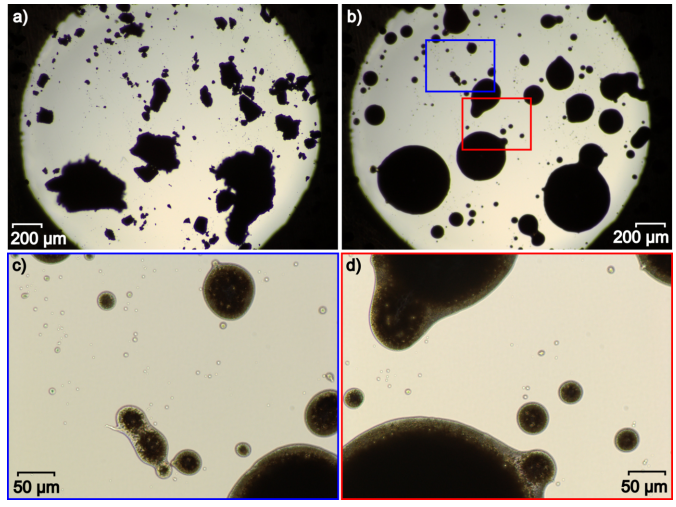

Figure 4
(*a*) $Ag_4(P_2O_6)$ powder before heating from 293 to 593 K, (*b*) after cooling from 593 to 293 K, along with zoomed (*c*) blue and (*d*) red areas (*cf* Fig. S5 in the supporting information).

VT-PXRD experiments, collected every 50 K between 300 and 850 K, have confirmed that $Ag_4(P_2O_6)$ is stable up to about 400 K (violet diffractograms in Fig. 5). At 450 K, decomposition begins and reflections from Ag appear (due to melting/decomposition and aggregation of the sample, the diffraction lines from the corundum sample holder also become visible; grey diffractograms in Fig. 5). On further heating, the intensities of the diffraction lines from metallic silver increase, and at 600 K, reflections from $Ag(PO_3)$ appear (blue diffractograms in Fig. 5) (Terebilenko *et al.*, 2011). This observation is consistent with the exothermic nature of the second peak on the DCS curve at about 620 K (crystallization). The crystalline $Ag(PO_3)$ formed in this way is stable up to a temperature of 700 K. Then, at about 750 K, it melts (literature m.p. 755–761 K; Osterheld & Mozer, 1973), which is accompanied by the disappearance of the diffraction pattern

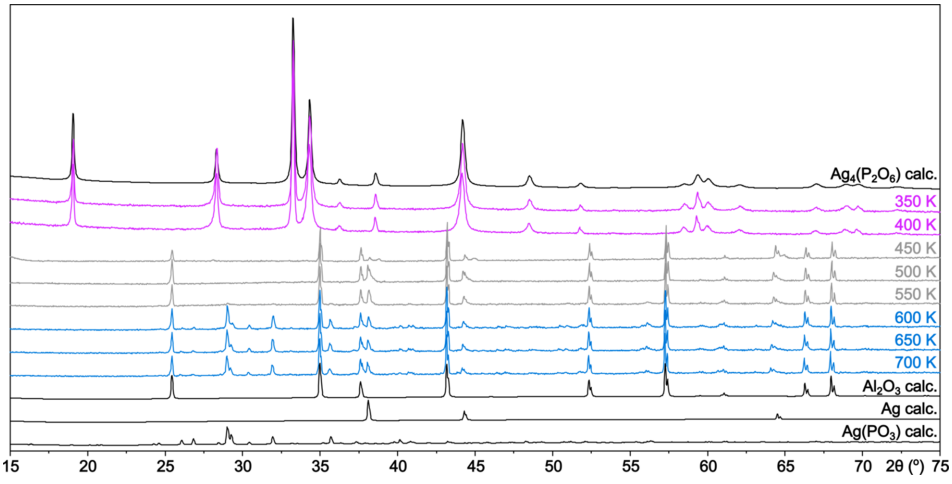

Figure 5
The variable-temperature powder X-ray diffraction (VT-PXRD) patterns for the sample of $Ag_4(P_2O_6)$ (2θ range 15–75°, recorded on heating every 50 K in the temperature range 350–700 K, shown from top to bottom). Calculated diffractograms are shown in black and experimental diffractograms are shown in violet, grey and blue.

in PXRD and the endothermic anomaly in the DSC curve at 750 K. The decomposition takes place as a redox process according to the equation:

$$Ag_4(P_2O_6) \rightarrow 2Ag(PO_3) + 2Ag,$$

and is consistent with the observations of Philipp (1883).

3.3. Average crystal structure

The average structure is the time- and space-averaged model derived from diffraction (Rietveld refinement), providing a perfect periodic symmetry that lacks local detail. Real structure refers to the instantaneous, accurate and local atomic positions (obtained from PDF, EXAFS, diffuse scattering), capturing all disorder, defects and thermal vibrations.

The crystal structure of silver hypodiphosphate, $Ag_4(P_2O_6)$, was determined using 3D ED. The average structural model obtained in this way was used for the Rietveld refinement of the PXRD data.

The average structure is hexagonal, described by $P6_3/mcm$ space-group symmetry, and isomorphous with the average structure of $Li_4(P_2S_6)$ (Mercier *et al.*, 1982). It should be noted that both known polymorphic modifications of $Ag_4(P_2S_6)$ crystallize as non-isomorphous with the $Ag_4(P_2O_6)$ structure types (Toffoli *et al.*, 1982; Toffoli *et al.*, 1983). The silver cations in $Ag_4(P_2O_6)$ form a three-dimensional substructure, in which hexagonal atomic ring 'layers' (perpendicular to [001]) can be distinguished. The 'layers' are arranged one above the other, forming channels along the *c*-axis direction. The metal centres are in close contact (Ag···Ag distances within the layers are 3.11 Å and Ag···Ag distances between the layers = $\frac{1}{2}c$ = 3.15 Å), which indicates argentophilic interactions (Schmidbaur & Schier, 2015). Hypodiphosphate anions, $P_2O_6^{4-}$, occupy the channels, with the P—P bond oriented along the the unique *c* axis. P atoms are disordered into two positions, each of which is 50% occupied, which means that the whole hypodiphosphate anion occupies two positions [shown as violet and blue in Fig. 6(*a*)]. O-atom positions are common to

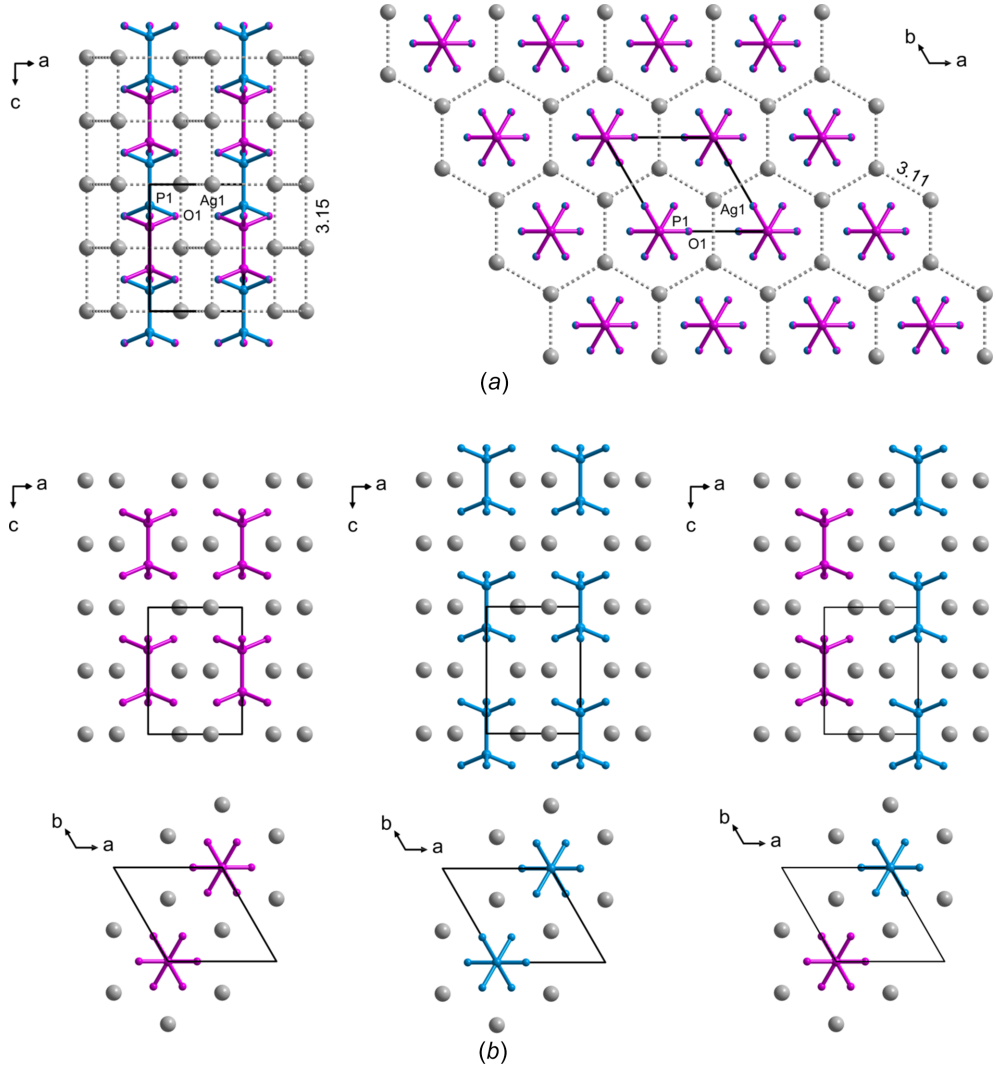

Figure 6
(*a*) Crystal structure packing views of $Ag_4(P_2O_6)$ along with (*b*) possible different mutual arrangements of the hypodiphosphate anions shown in violet and blue colours. The Ag···Ag distances in part (*a*) are given in Å.

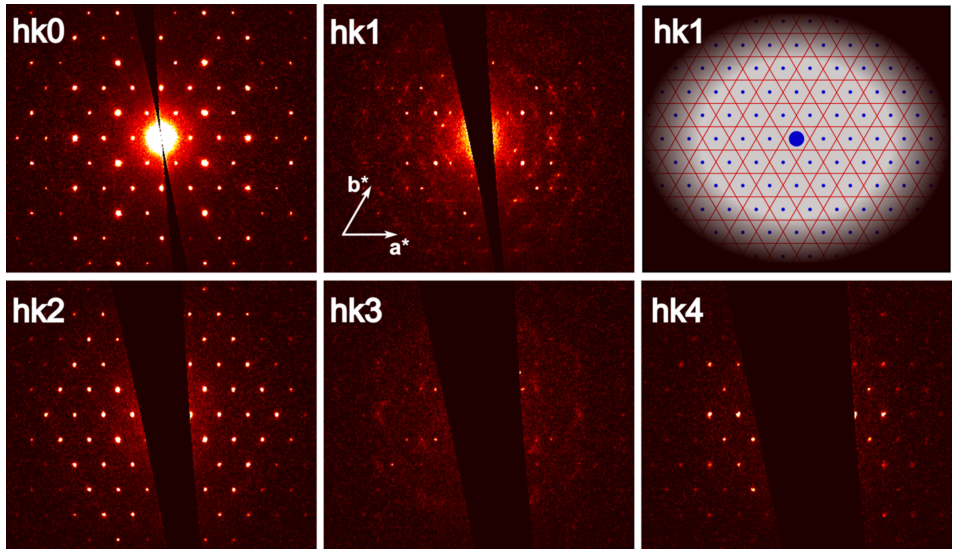

Figure 7
Ewald sphere reconstructions with diffuse scattering seen on *hkl* layers with $l = 1$ and $l = 3$, along with the schematic view of the diffuse streaks shown as red lines, Bragg reflections as small blue dots and the primary beam as a large blue dot (*cf* Fig. S7 in the supporting information).

both disorder components and create an octahedral coordination environment for the silver cations (Fig. S6). Hypodiphosphate anions are stacked into columns along the *c*-axis direction. Each column is chemically and structurally identical, but neighbouring columns may have P—P bonds on the same or on different levels [compare with the example arrangements of adjacent columns shown in Fig. 6(*b*)].

3.4. Diffuse scattering

The observed diffuse scattering (DS) lines on the *hkl* reciprocal planes shown in Fig. 7 (where l is odd, $l = 2m + 1$) appear midway between Bragg reflections along the a^*, b^* and a^*–b^* directions. This suggests short-range order in the crystal, with local doubling of the unit-cell parameters along the [100], [010] and [110] directions. The origin of this effect is in the occupational disorder at the P-site, which is half-occupied. However, along the *c*-axis direction, the P atoms are perfectly ordered due to the nature of the structure, resulting in the long-range order along this axis.

In contrast, along the [100], [010] and [110] directions, the atomic arrangement allows for multiple configurations, but still tends toward a local ordering. This local ordering forms ordered layers perpendicular to these three directions, and the diffuse scattering lines observed between Bragg peaks are a direct consequence of these short-range atomic correlations. The overall structure retains long-range order in the *c*-axis direction, but exhibits short-range order along the other directions, providing insight into the atomic arrangements in the disordered regions.

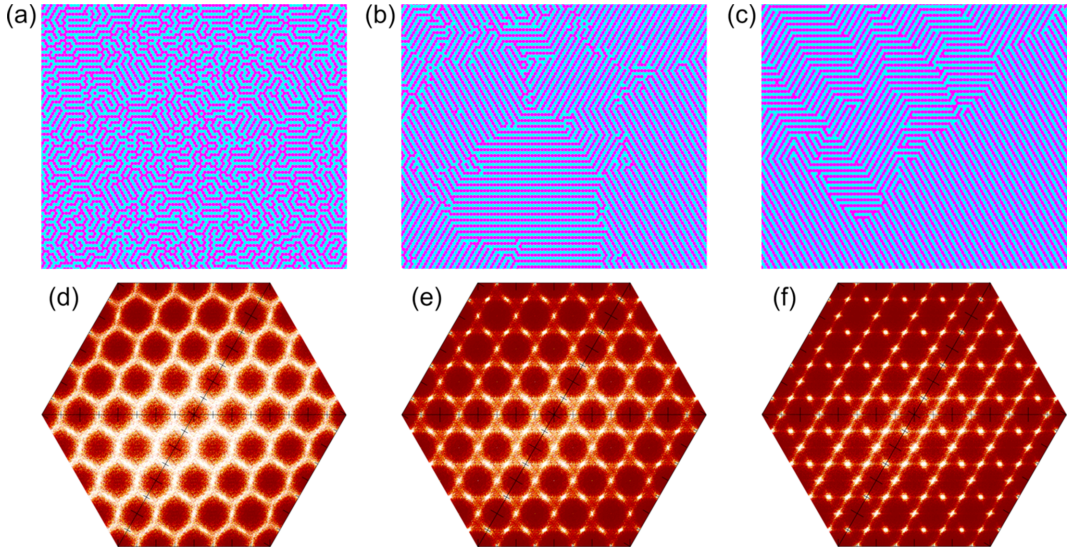

Figure 8
Example realizations of the Ising model with $J_1 = -5.0$ and varying values of J_2: (*a*) $J_2 = 0.0$, (*b*) $J_2 = -0.3$ and (*c*) $J_2 = -3.0$. Corresponding calculated *hk*1 sections of reciprocal space are shown in parts (*d*)–(*f*), respectively.

To propose a model of short-range order, it is essential to consider the concept of 'geometric frustration'. This well-established idea has been applied previously to explain diffuse scattering effects in various crystal systems (Welberry *et al.*, 2011). We adopted a similar approach to investigate the spatial distribution of two distinct types of scatterers located on the triangular lattice of the *ab* plane in a hexagonal crystal. In our system, two possible anion configurations exist – designated as **A** and **B** (represented in blue and violet in Fig. 6). When an alternating arrangement of **A** and **B** is energetically favourable, such ordering is readily achievable on a square lattice but inherently frustrated on a triangular one. Specifically, when two sides of a triangle are occupied by alternating anions (**A** and **B**), the third must necessarily result in a like-pair (**AA** or **BB**), making perfect alternation geometrically impossible.

To implement such a model, Monte Carlo (MC) simulations based on the Ising model were employed. This approach has been used successfully in numerous studies to model various types of disorder in crystals (Welberry, 2004; Welberry *et al.*, 2011; Komornicka *et al.*, 2014; Bednarchuk *et al.*, 2017; Kowalska *et al.*, 2021). Simulations were performed for a series of cases using correlation parameters for both nearest-neighbour (J_1) and next-nearest-neighbour (J_2) interactions. The correlations were defined such that when $J_i < 0$, neighbouring sites tend to differ in type.

The calculated models consist only of P ions, as the remaining atoms in the structure are fully ordered and do not contribute to the observed diffuse scattering effects. Three examples are presented in Fig. 8. In these simulations, the value of J_1 was fixed at −5.0, while J_2 was varied. Figs. 8(*a*)–(*c*) show the lattice configurations corresponding to each model, providing an overview of the spatial arrangements. The associated diffraction patterns (*hk*1 section) calculated from these configurations, are shown in Figs. 8(*d*)–(*f*).

In Fig. 8(*d*), with $J_2 = 0$, the diffuse scattering appears as featureless diffuse rings. Introducing a small negative value for J_2 (−0.3) leads to narrowing of the diffuse features and the appearance of distinct intensity enhancements midway between pairs of Bragg peaks [Fig. 8(*e*)]. Further decreasing J_2 to −3.0 results in the weakening of diffuse streaks and a marked increase in additional intensity maxima [Fig. 8(*f*)]. Fig. 8(*e*) shows characteristics very similar to the observed patterns; therefore, the distribution in Fig. 8(*b*) can be considered the most representative of the short-range order present in the studied nanocrystal. Ewald sphere reconstructions based on the selected model, corresponding to those presented in Fig. 7, are shown in Fig. S8 in the supporting information.

4. Conclusions

The average crystal structure of silver hypodiphosphate, $Ag_4(P_2O_6)$, was determined from 3D electron diffraction and Rietveld fitting against PXRD data. The hexagonal structure is characterized by the statistical disorder of hypodiphosphate anions, perfectly correlated along a unique axis direction and geometrically frustrated in the *ab* plane. Electron diffraction data revealed diffuse scattering between Bragg peaks on *hkl* layers with odd values of *l*, that originates from the presence of locally correlated anion arrangements, incompatible with long-range periodicity. Simulations using a frustrated Ising model reproduce the key features of the experimental data, providing insight into the nature of short-range order in the crystal.

Acknowledgements

This research was performed under a cooperation agreement between Rigaku Polska Sp. z o.o. and the University of Wrocław (agreement No. 1/2021).

Conflict of interest

There are no conflicts of interest.

Data availability

The published raw data, along with any supporting information not included in the article, is available from the authors upon reasonable request.

References

Bednarchuk, T. J., Kowalska, D., Kinzhybalo, V. & Wołcyrz, M. (2017). *Acta Cryst.* B**73**, 337–346.
Brandenburg, K. (2022). *DIAMOND*. Crystal Impact GbR, Bonn, Germany.
Degen, T., Sadki, M., Bron, E., König, U. & Nénert, G. (2014). *Powder Diffr.* **29**, S13–S18.
Dietrich, C., Sadowski, M., Sicolo, S., Weber, D. A., Sedlmaier, S. J., Weldert, K. S., Indris, S., Albe, K., Janek, J. & Zeier, W. G. (2016). *Chem. Mater.* **28**, 8764–8773.
Dolomanov, O. V., Bourhis, L. J., Gildea, R. J., Howard, J. A. K. & Puschmann, H. (2009). *J. Appl. Cryst.* **42**, 339–341.
Gjikaj, M. & Wu, P. (2014). *Z. Anorg. Allg. Chem.* **640**, 189–194.
Gjikaj, M., Wu, P. & Brockner, W. (2012). *Z. Anorg. Allg. Chem.* **638**, 2144–2149.
Gjikaj, M., Wu, P. & Brockner, W. (2014). *Z. Anorg. Allg. Chem.* **640**, 379–384.
Grimmer, A.-R. (1978). *Z. Chem.* **18**, 109–110.
Haase, M. & Gjikaj, M. (2017). *Z. Anorg. Allg. Chem.* **643**, 962–967.
Haase, M. & Gjikaj, M. (2018). *Z. Anorg. Allg. Chem.* **644**, 497–503.
Hogrefe, K., Gadermaier, B., Schneider, Ch., Bette, S., Lotsch, B. V. & Wilkening, H. M. R. (2025). *J. Am. Chem. Soc.* **147**, 28799–28809.
Hood, Z. D., Kates, C., Kirkham, M., Adhikari, S., Liang, C. & Holzwarth, N. A. W. (2016). *Solid State Ionics* **284**, 61–70.
Ito, Sh., White, F. J., Okunishi, E., Aoyama, Y., Yamano, A., Sato, H., Ferrara, J. D., Jasnowski, M. & Meyer, M. (2021). *CrystEngComm* **23**, 8622–8630.
Joly, A. (1885). *Compt. Rend.* **101**, 1058–1061.
Kabekkodu, S. & Blanton, T. (2024). *Acta Cryst.* B**80**, 364–369.
Kabekkodu, S. N., Dosen, A. & Blanton, T. N. (2024). *Powder Diffr.* **39**, 47–59.
Keen, D. & Goodwin, A. (2015). *Nature* **521**, 303–309.
Kinzhybalo, V., Mermer, A., Lis, T. & Starynowicz, P. (2013). *Acta Cryst.* B**69**, 344–355.
Kinzhybalo, V., Otręba, M., Ślepokura, K. & Lis, T. (2021). *Wiad. Chem.* **75**, 423–466.

Kinzhybalo, V., Wojciechowski, J., Szklarz, P., Piecha-Bisiorek, A., Otręba, M., Siczek, M. & Ślepokura, K. (2024). *J. Mater. Chem. C* **12**, 11347–11351.
Komornicka, D., Wołcyrz, M. & Pietraszko, A. (2014). *Cryst. Growth Des.* **14**, 5784–5793.
Kowalska, D. A., Kinzhybalo, V., Slyvka, Yu. I. & Wołcyrz, M. (2021). *Acta Cryst.* B**77**, 241–248.
Li, Y., Hood, Z. D. & Holzwarth, N. A. W. (2020). *Phys. Rev. Mater.* **4**, 045406.
Mercier, R., Malugani, J. P., Fahys, B., Douglande, J. & Robert, G. (1982). *J. Solid State Chem.* **43**, 151–162.
Neuberger, S., Culver, S. P., Eckert, H., Zeier, W. G. & Schmedt auf der Günne, J. (2018). *Dalton Trans.* **47**, 11691–11695.
Neuberger, S., Mathew, N., Adediwura, S. C., Sanchez, H. J. C. & Schmedt auf der Günne, J. (2025). *Dalton Trans.* **54**, 11996–12005.
Osterheld, R. K. & Mozer, T. J. (1973). *J. Inorg. Nucl. Chem.* **35**, 3463–3465.
Otręba, M., Kinzhybalo, V., Sokołowska, A. M., Lipiński, R., Szklarz, P., Piecha-Bisiorek, A. & Ślepokura, K. A. (2026). *Acta Cryst.* B**82**, 209–223.
Oxley, B. M., Lee, K.-H., Ie, T. S., Lee, J. M., Waters, M. J., Rondinelli, J. M., Jang, J. I. & Kanatzidis, M. G. (2023). *Chem. Mater.* **35**, 7322–7332.
Philipp, J. (1883). *Ber. Dtsch Chem. Ges.* **16**, 749–752.
Proffen, Th. & Neder, R. B. (1997). *J. Appl. Cryst.* **30**, 171–175.
Rigaku OD (2022). *CrysAlis PRO*. Rigaku Oxford Diffraction Ltd, Yarnton, Oxfordshire, UK.
Saha, A., Nia, S. S. & Rodríguez, J. A. (2022). *Chem. Rev.* **122**, 13883–13914.
Salzer, Th. (1877). *Justus Liebigs Ann. Chem.* **187**, 322–340.
Salzer, Th. (1886). *Justus Liebigs Ann. Chem.* **232**, 114–121.
Sänger, A. (1886). *Justus Liebigs Ann. Chem.* **232**, 1–42.
Schmidbaur, H. & Schier, A. (2015). *Angew. Chem. Int. Ed.* **54**, 746–784.
Schmidt, E. M., Klar, P. B., Krysiak, Y., Svora, P., Goodwin, A. L. & Palatinus, L. (2023). *Nat. Commun.* **14**, 6512.
Scholz, T., Schneider, Ch., Eger, R., Duppel, V., Moudrakovski, I., Schulz, A., Nuss, J. & Lotsch, B. V. (2021). *J. Mater. Chem. A* **9**, 8692–8703.
Scholz, T., Schneider, Ch., Terban, M. W., Deng, Z., Eger, R., Etter, M., Dinnebier, R. E., Canepa, P. & Lotsch, B. V. (2022). *ACS Energy Lett.* **7**, 1403–1411.
Sheldrick, G. M. (2015). *Acta Cryst.* C**71**, 3–8.
Ślepokura, K. A., Kurowska, P., Budzikur-Maciąg, D. & Kinzhybalo, V. (2025). *Acta Cryst.* B**81**, 407–417.
Stamminger, A. R., Ziebarth, B., Mrovec, M., Hammerschmidt, Th. & Drautz, R. (2020). *RSC Adv.* **10**, 10715–10722.
Starynowicz, P., Ślepokura, K. A., Kurowska, P. & Kinzhybalo, V. (2025). *Acta Cryst.* B**81**, 135–145.
Szafranowska, B., Ślepokura, K. & Lis, T. (2012). *Acta Cryst.* C**68**, i71–i82.
Szklarz, P., Chański, M., Ślepokura, K. & Lis, T. (2011). *Chem. Mater.* **23**, 1082–1084.
Terebilenko, K. V., Zatovsky, I. V., Ogorodnyk, I. V., Baumer, V. N. & Slobodyanik, N. S. (2011). *Acta Cryst.* E**67**, i22.
Toffoli, P., Khodadad, P. & Rodier, N. (1983). *Acta Cryst.* C**39**, 1485–1488.
Toffoli, P., Michelet, A., Khodadad, P. & Rodier, N. (1982). *Acta Cryst.* B**38**, 706–710.
Welberry, T. R. (2004). *Diffuse X-ray Scattering and Models of Disorder*. IUCr Monographs on Crystallography. Oxford University Press.
Welberry, T. R., Heerdegen, A. P., Goldstone, D. C. & Taylor, I. A. (2011). *Acta Cryst.* B**67**, 516–524.
Wolf, L. & Jung, W. (1931). *Z. Anorg. Allg. Chem.* **201**, 347–352.
Wu, P., Pook, N.-P. & Gjikaj, M. (2015). *Z. Anorg. Allg. Chem.* **641**, 1755–1761.
Wu, P., Wiegand, Th., Eckert, H. & Gjikaj, M. (2012). *J. Solid State Chem.* **194**, 212–218.
Yahia, H. B., Motohashi, K., Sakuda, A., Hayashi, A. & Mori, S. (2023). *Z. Kristallogr. Cryst. Mater.* **238**, 209–216.
Yoza, N. & Ohashi, S. (1965). *Bull. Chem. Soc. Jpn* **38**, 1408–1409.

supporting information

Acta Cryst. (2026). C**82**, 277-284 [https://doi.org/10.1107/S2053229626005012]

Diffuse scattering in silver hypodiphosphate, $Ag_4(P_2O_6)$, probed by 3D ED

Vasyl Kinzhybalo, Jakub Wojciechowski, Dorota A. Kowalska, Vladyslav Maliuzhenko and Katarzyna A. Ślepokura

Computing details

Tetrasilver hypodiphosphate (exp_7626_kinem)

Crystal data

$Ag_4(P_2O_6)$
M_r = 589.42
Hexagonal, $P6_3/mcm$
a = 5.39128 (7) Å
c = 6.30229 (9) Å
V = 158.64 (1) Å^3
Z = 1
$F(000)$ = -29
D_x = 6.170 Mg m^{-3}
μ = 0.000 mm^{-1}
T = 298 K

Data collection

725 measured reflections
64 independent reflections
60 reflections with $I > 2\sigma(I)$
R_{int} = 0.128
θ_{max} = 0.9°, θ_{min} = 0.2°
h = −6→6
k = −6→6
l = −7→6

Refinement

Refinement on F^2
Least-squares matrix: full
$R[F^2 > 2\sigma(F^2)]$ = 0.116
$wR(F^2)$ = 0.400
S = 2.09
64 reflections
11 parameters
0 restraints
Primary atom site location: iterative
$w = 1/[\sigma^2(F_o^2) + (0.160P)^2 + 0.050P]$ where $P = (F_o^2 + 2F_c^2)/3$
$(\Delta/\sigma)_{max} < 0.001$
$\Delta\rho_{max}$ = 0.33 e Å^{-3}
$\Delta\rho_{min}$ = −0.29 e Å^{-3}
Extinction correction: SHELXL2014 (Sheldrick, 2015), $Fc^*=kFc[1+0.001xFc^2\lambda^3/\sin(2\theta)]^{-1/4}$
Extinction coefficient: 35470 (58)

Special details

Geometry. All esds (except the esd in the dihedral angle between two l.s. planes) are estimated using the full covariance matrix. The cell esds are taken into account individually in the estimation of esds in distances, angles and torsion angles; correlations between esds in cell parameters are only used when they are defined by crystal symmetry. An approximate (isotropic) treatment of cell esds is used for estimating esds involving l.s. planes.

Fractional atomic coordinates and isotropic or equivalent isotropic displacement parameters (Å^2)

	x	*y*	*z*	U_{iso}*/U_{eq}	Occ. (<1)
Ag1	0.6667	0.3333	0.0000	0.045 (4)	
P1	0.0000	0.0000	0.171 (9)	0.032 (12)	0.5

O1	0.276 (3)	0.0000	0.2500	0.040 (8)

Atomic displacement parameters (Å²)

	U^{11}	U^{22}	U^{33}	U^{12}	U^{13}	U^{23}
Ag1	0.039 (4)	0.039 (4)	0.057 (9)	0.019 (2)	0.000	0.000
P1	0.020 (9)	0.020 (9)	0.05 (4)	0.010 (5)	0.000	0.000
O1	0.012 (6)	0.024 (10)	0.09 (2)	0.012 (5)	0.000	0.000

Geometric parameters (Å, º)

P1—P1^{i}	0.99 (11)	P1—O1^{iv}	1.57 (2)
P1—P1^{ii}	2.16 (11)	P1—O1^{v}	1.57 (2)
P1—O1^{iii}	1.57 (2)	P1—O1^{i}	1.57 (2)
P1—O1	1.57 (2)	O1—P1^{i}	1.57 (2)
P1^{i}—P1—P1^{ii}	180.000 (13)	O1^{v}—P1—O1	110.5 (19)
P1^{i}—P1—O1^{iv}	71.6 (19)	O1^{iv}—P1—O1^{iii}	110.5 (19)
P1^{i}—P1—O1^{iii}	71.6 (19)	O1^{i}—P1—O1^{iii}	0.0
P1^{i}—P1—O1^{v}	71.6 (19)	O1^{iv}—P1—O1^{v}	110.5 (19)
P1^{i}—P1—O1^{i}	71.6 (19)	O1^{v}—P1—O1^{iii}	110.5 (19)
P1^{i}—P1—O1	71.6 (19)	O1^{iii}—P1—O1	0.0
O1^{iii}—P1—P1^{ii}	108.4 (19)	O1^{iv}—P1—O1	110.5 (19)
O1^{v}—P1—P1^{ii}	108.4 (19)	O1^{iv}—P1—O1^{i}	110.5 (19)
O1^{i}—P1—P1^{ii}	108.4 (19)	O1^{v}—P1—O1^{i}	110.5 (19)
O1^{iv}—P1—P1^{ii}	108.4 (19)	O1^{i}—P1—O1	0.0
O1—P1—P1^{ii}	108.4 (19)	P1—O1—P1^{i}	37 (4)
P1^{ii}—P1—O1—P1^{i}	180.000 (5)	O1^{v}—P1—O1—P1^{i}	61 (2)
O1^{iv}—P1—O1—P1^{i}	−61 (2)	O1^{i}—P1—O1—P1^{i}	0 (100)
O1^{iii}—P1—O1—P1^{i}	0 (100)		

Symmetry codes: (i) *x*, *y*, −*z*+1/2; (ii) −*x*, −*y*, −*z*; (iii) *x*−*y*, −*y*, −*z*+1/2; (iv) −*x*+*y*, −*x*, *z*; (v) −*y*, *x*−*y*, *z*.

(exp_7626_dynam)

Crystal data

$Ag_4O_6P_2$
M_r = 589.42
Hexagonal, $P6_3/mcm$
a = 5.39128 (7) Å
c = 6.30229 (9) Å
V = 158.64 (1) Å³
Z = 1
F(000) = 298.006
D_x = 6.170 Mg m^{-3}
Synchrotron radiation, λ = 0.02510 Å
μ = 0.05 mm^{-1}
T = 298 K

Data collection

1500 measured reflections
725 independent reflections
479 reflections with $I \geq 2u(I)$
R_{int} = 0.155
θ_{max} = 0.9°, θ_{min} = 0.2°
h = −8→8
k = −8→8
l = −9→9

Refinement

Refinement on F^2
Least-squares matrix: full
$R[F^2 > 2\sigma(F^2)] = 0.122$
$wR(F^2) = 0.281$
$S = 1.61$
64 reflections
10 parameters
0 restraints
0 constraints
Primary atom site location: iterative
$w = 1/[\sigma^2(F_o^2) + (0.050P)^2]$
where $P = (F_o^2 + 2F_c^2)/3$
$(\Delta/\sigma)_{max} = -0.0003$
$\Delta\rho_{max} = 16.02$ e Å^{-3}
$\Delta\rho_{min} = -9.94$ e Å^{-3}

Fractional atomic coordinates and isotropic or equivalent isotropic displacement parameters (Å²)

	x	*y*	*z*	U_{iso}*/U_{eq}	Occ. (<1)
Ag1	0.666667	0.333333	0.0	0.0389 (10)	
P1	0.0	0.0	0.1784 (19)	0.022 (5)	0.500000
O1	0.2706 (10)	0.0	0.25	0.028 (2)	

Atomic displacement parameters (Å²)

	U^{11}	U^{22}	U^{33}	U^{12}	U^{13}	U^{23}
Ag1	0.0402 (10)	0.0402 (10)	0.036 (3)	0.0201 (5)	−0.000000	0.000000
P1	0.013 (2)	0.013 (2)	0.041 (14)	0.0064 (11)	−0.000000	0.000000
O1	0.020 (2)	0.014 (3)	0.048 (8)	0.0068 (14)	−0.000000	0.000000

Geometric parameters (Å, º)

Ag1—Ag1^{i}	3.1127 (1)	Ag1—O1^{ix}	2.536 (3)
Ag1—Ag1^{ii}	3.1512 (1)	Ag1—O1	2.536 (3)
Ag1—Ag1^{iii}	3.1127 (1)	Ag1—O1^{x}	2.536 (3)
Ag1—Ag1^{iv}	3.1512 (1)	O1—P1	1.527 (7)
Ag1—Ag1^{v}	3.1127 (1)	O1—P1^{xi}	1.527 (7)
Ag1—O1^{vi}	2.536 (3)	P1—P1^{xi}	0.90 (2)
Ag1—O1^{vii}	2.536 (3)	P1—P1^{xii}	2.25 (2)
Ag1—O1^{viii}	2.536 (3)		
Ag1^{iii}—Ag1—Ag1^{v}	120.0	O1^{ix}—Ag1—O1^{vii}	104.30 (10)
Ag1^{iii}—Ag1—Ag1^{ii}	90.0	O1^{vii}—Ag1—O1^{viii}	85.48 (7)
O1^{vii}—Ag1—Ag1^{v}	83.37 (10)	O1^{vi}—Ag1—O1	104.30 (10)
O1^{ix}—Ag1—Ag1^{ii}	51.60 (5)	O1^{ix}—Ag1—O1	85.48 (7)
O1^{ix}—Ag1—Ag1^{v}	136.80 (9)	O1^{x}—Ag1—O1^{viii}	104.30 (10)
O1^{x}—Ag1—Ag1^{ii}	51.60 (5)	Ag1^{i}—O1—Ag1	75.70 (10)
O1^{x}—Ag1—Ag1^{iii}	83.37 (10)	Ag1^{ii}—O1—Ag1	76.80 (10)
O1^{ix}—Ag1—Ag1^{iii}	52.15 (5)	Ag1^{i}—O1—Ag1^{xiii}	76.80 (10)
O1^{vi}—Ag1—Ag1^{ii}	128.40 (5)	Ag1^{xiii}—O1—Ag1	121.6 (2)
O1^{vii}—Ag1—Ag1^{ii}	128.40 (5)	Ag1^{ii}—O1—Ag1^{i}	121.6 (2)
O1^{viii}—Ag1—Ag1^{v}	52.15 (5)	Ag1^{ii}—O1—Ag1^{xiii}	75.70 (10)
O1—Ag1—Ag1^{v}	83.37 (10)	P1—O1—Ag1^{ii}	130.5 (3)
O1^{viii}—Ag1—Ag1^{iii}	136.80 (9)	P1^{xi}—O1—Ag1^{xiii}	106.4 (3)
O1^{x}—Ag1—Ag1^{v}	52.15 (5)	P1—O1—Ag1^{xiii}	130.5 (3)

O1^{viii}—Ag1—Ag1^{ii}	128.40 (5)	P1^{xi}—O1—Ag1	130.5 (3)
O1—Ag1—Ag1^{iii}	136.80 (9)	P1^{xi}—O1—Ag1^{ii}	106.4 (3)
O1^{vii}—Ag1—Ag1^{iii}	52.15 (5)	P1^{xi}—O1—Ag1^{i}	130.5 (3)
O1^{vi}—Ag1—Ag1^{iii}	83.37 (10)	P1—O1—Ag1	106.4 (3)
O1—Ag1—Ag1^{ii}	51.60 (5)	P1—O1—Ag1^{i}	106.4 (3)
O1^{vi}—Ag1—Ag1^{v}	136.80 (9)	P1^{xi}—O1—P1	34.4 (9)
O1^{viii}—Ag1—O1	86.40 (19)	O1^{xiv}—P1—O1	111.7 (4)
O1^{vi}—Ag1—O1^{viii}	85.48 (7)	O1^{xv}—P1—O1	111.7 (4)
O1^{x}—Ag1—O1^{ix}	85.48 (7)	O1^{xiv}—P1—O1^{xv}	111.7 (4)
O1^{ix}—Ag1—O1^{viii}	166.7 (2)	P1^{xi}—P1—O1	72.8 (4)
O1^{x}—Ag1—O1^{vii}	86.40 (19)	P1^{xii}—P1—O1^{xiv}	107.2 (4)
O1^{vi}—Ag1—O1^{x}	166.7 (2)	P1^{xii}—P1—O1^{xv}	107.2 (4)
O1^{x}—Ag1—O1	85.48 (7)	P1^{xi}—P1—O1^{xiv}	72.8 (4)
O1^{vii}—Ag1—O1	166.7 (2)	P1^{xi}—P1—O1^{xv}	72.8 (4)
O1^{vi}—Ag1—O1^{ix}	86.40 (19)	P1^{xii}—P1—O1	107.2 (4)
O1^{vi}—Ag1—O1^{vii}	85.48 (7)		

Ag1—O1—P1—O1^{xv}	−77.34 (18)	O1—P1—O1^{xiv}—Ag1^{xli}	−156.9 (5)
Ag1^{ix}—O1—P1—O1^{xv}	−77.34 (18)	O1—P1^{xi}—O1^{xxix}—Ag1^{xlii}	116.7 (3)
Ag1^{x}—O1—P1—O1^{xv}	−77.34 (18)	O1—P1—O1^{xv}—Ag1^{xliii}	−116.7 (3)
Ag1—O1^{ix}—P1^{xvi}—O1^{xvii}	−9.12 (6)	O1—P1^{xi}—O1^{xxvi}—Ag1^{xliv}	−116.7 (3)
Ag1^{xviii}—O1—P1—O1^{xv}	116.7 (6)	O1^{xxix}—P1—O1—Ag1	−77.3 (6)
Ag1—O1^{vi}—P1^{xix}—O1^{xx}	156.9 (3)	O1—P1—O1^{xv}—Ag1^{xlv}	77.3 (6)
Ag1—O1^{ix}—P1^{xvi}—O1^{xxi}	116.7 (6)	O1—P1^{xi}—O1^{xxix}—Ag1^{xlvi}	−156.9 (5)
Ag1—O1—P1—O1^{xiv}	156.9 (3)	O1—P1^{xi}—O1^{xxix}—Ag1^{xlvii}	9.1 (9)
Ag1—O1^{x}—P1^{xxii}—O1^{xxiii}	116.7 (6)	O1^{xxvi}—P1—O1—Ag1	156.9 (5)
Ag1—O1^{x}—P1^{xxii}—O1^{xxiv}	−9.12 (6)	O1—P1—O1^{xiv}—Ag1^{xiv}	−77.3 (6)
Ag1—O1^{vi}—P1^{xix}—O1^{xxv}	−77.34 (18)	O1—P1^{xi}—O1^{xxvi}—Ag1^{xlviii}	77.3 (6)
Ag1—O1—P1^{xi}—O1^{xxvi}	116.7 (6)	O1—P1—O1^{xv}—Ag1^{xlix}	−9.1 (9)
Ag1—O1^{viii}—P1^{xxvii}—O1^{xii}	−77.34 (18)	O1—P1^{xi}—O1^{xxvi}—P1	−62.9 (6)
Ag1^{x}—O1—P1—O1^{xiv}	156.9 (3)	O1—P1—O1^{xv}—P1^{xxix}	−62.9 (6)
Ag1—O1^{viii}—P1^{xxvii}—O1^{xxviii}	156.9 (3)	O1—P1^{xi}—O1^{xxix}—P1	62.9 (6)
Ag1—O1—P1^{xi}—O1^{xxix}	−9.12 (6)	O1—P1—O1^{xiv}—P1^{xxvi}	62.9 (6)
Ag1^{xiii}—O1—P1—O1^{xv}	116.7 (6)	O1—P1—P1^{xi}—O1^{xxix}	120.0
Ag1^{ix}—O1—P1—O1^{xiv}	156.9 (3)	O1—P1^{xi}—P1—O1^{xv}	−120.0
Ag1^{xiii}—O1—P1—O1^{xiv}	−9.12 (6)	O1—P1—P1^{xi}—O1^{xxvi}	−120.0
Ag1^{xxx}—O1—P1—O1^{xv}	116.7 (6)	O1—P1^{xi}—P1—O1^{xiv}	120.0
Ag1—O1^{vii}—P1^{xxxi}—O1^{xxxii}	−77.34 (18)	P1—O1—P1^{xi}—O1^{xxix}	−62.9 (3)
Ag1^{xviii}—O1—P1—O1^{xiv}	−9.12 (6)	P1—O1—P1^{xi}—O1^{xxvi}	62.9 (3)
Ag1^{xxx}—O1—P1—O1^{xiv}	−9.12 (6)	P1—O1^{xv}—P1^{xxix}—O1^{xxvi}	−62.9 (3)
Ag1—O1^{vii}—P1^{xxxi}—O1^{xxxiii}	156.9 (3)	P1—O1^{xiv}—P1^{xxvi}—O1	−62.9 (3)
Ag1—O1—P1^{xi}—P1^{xxxiv}	−126.2 (3)	P1—O1^{xiv}—P1^{xxvi}—O1^{xxix}	62.9 (3)
Ag1^{xiii}—O1—P1—P1^{xi}	53.8 (3)	P1—O1^{xv}—P1^{xxix}—O1	62.9 (3)
Ag1^{x}—O1—P1^{xi}—P1	53.8 (3)	P1—O1^{xv}—P1^{xxix}—P1^{l}	180.0
Ag1—O1—P1^{xi}—P1	53.8 (3)	P1—O1—P1^{xi}—P1^{xxxiv}	180.0
Ag1^{xiii}—O1—P1^{xi}—P1	−140.24 (9)	P1—O1^{xiv}—P1^{xxvi}—P1^{xxx}	180.0
Ag1^{xxx}—O1—P1—P1^{xi}	53.8 (3)	P1^{xi}—P1—O1—Ag1^{ii}	−53.8 (3)
Ag1—O1—P1—P1^{xii}	39.76 (9)	P1—P1^{xii}—O1^{xxvii}—Ag1^{li}	126.2 (3)

Ag1^{xxx}—O1—P1^{xi}—P1	−140.24 (9)	P1—P1^{xi}—O1^{xxix}—Ag1^{xlii}	53.8 (3)
Ag1^{ix}—O1—P1—P1^{xi}	−140.24 (9)	P1—P1^{xi}—O1^{xxix}—Ag1^{xlvii}	−53.8 (3)
Ag1^{ix}—O1—P1—P1^{xii}	39.76 (9)	P1^{xxix}—P1—O1—Ag1	−140.24 (8)
Ag1—O1^{ix}—P1^{xvi}—P1^{xviii}	−126.2 (3)	P1—P1^{xii}—O1^{xxviii}—Ag1^{lii}	126.2 (3)
Ag1^{x}—O1—P1—P1^{xi}	−140.24 (9)	P1—P1^{xii}—O1^{xxvii}—Ag1^{liii}	−126.2 (3)
Ag1^{xxx}—O1—P1—P1^{xii}	−126.2 (3)	P1^{xii}—P1—O1—Ag1^{ii}	126.2 (3)
Ag1—O1^{x}—P1^{xxii}—P1^{xxxv}	−126.2 (3)	P1^{xxviii}—P1—O1—Ag1	39.76 (8)
Ag1^{xviii}—O1—P1—P1^{xi}	53.8 (3)	P1—P1^{xi}—O1^{xxvi}—Ag1^{xl}	53.8 (3)
Ag1^{xviii}—O1—P1—P1^{xii}	−126.2 (3)	P1—P1^{xii}—O1^{xxviii}—Ag1^{xliv}	−39.76 (8)
Ag1—O1^{vi}—P1^{xix}—P1^{xxxvi}	39.76 (9)	P1^{xxvii}—P1—O1—Ag1	39.76 (8)
Ag1—O1^{viii}—P1^{xxvii}—P1	39.76 (9)	P1—P1^{xi}—O1^{xxix}—Ag1^{xlvi}	140.24 (8)
Ag1^{xviii}—O1—P1^{xi}—P1	−140.24 (9)	P1—P1^{xi}—O1^{xxvi}—Ag1^{xlviii}	140.24 (8)
Ag1^{xiii}—O1—P1—P1^{xii}	−126.2 (3)	P1^{xi}—P1—O1—Ag1^{i}	140.24 (8)
Ag1—O1^{vii}—P1^{xxxi}—P1^{xxxvii}	39.76 (9)	P1^{xii}—P1—O1—Ag1^{i}	−39.76 (8)
Ag1—O1—P1—P1^{xi}	−140.24 (9)	P1—P1^{xi}—O1^{xxvi}—Ag1^{xliv}	−53.8 (3)
Ag1^{ix}—O1—P1^{xi}—P1	53.8 (3)	P1^{xxvi}—P1—O1—Ag1	−140.24 (8)
Ag1^{x}—O1—P1—P1^{xii}	39.76 (9)	P1—P1^{xii}—O1^{xxvii}—Ag1^{xlvii}	−39.76 (8)
O1—P1—O1^{xv}—Ag1^{xv}	156.9 (5)	P1—P1^{xii}—O1^{xxviii}—Ag1^{liv}	−126.2 (3)
O1—P1—O1^{xiv}—Ag1^{xxxviii}	116.7 (3)	P1—P1^{xii}—O1^{xxviii}—P1^{lv}	180.0
O1—P1—O1^{xiv}—Ag1^{xxxix}	9.1 (9)	P1—P1^{xii}—O1^{xxvii}—P1^{viii}	−180.0
O1—P1^{xi}—O1^{xxvi}—Ag1^{xl}	−9.1 (9)	P1^{xii}—P1—O1—P1^{xi}	180.0

Symmetry codes: (i) −*x*+1, −*y*, −*z*; (ii) −*x*+*y*+1, −*x*+1, −*z*+1/2; (iii) −*x*+2, −*y*+1, −*z*; (iv) −*x*+*y*+1, −*x*+1, −*z*−1/2; (v) −*x*+1, −*y*+1, −*z*; (vi) −*x*+1, −*y*, *z*−1/2; (vii) *y*+1, −*x*+*y*+1, *z*−1/2; (viii) *x*−*y*, *x*, *z*−1/2; (ix) −*y*+1, *x*−*y*, *z*; (x) −*x*+*y*+1, −*x*+1, *z*; (xi) *x*−*y*, −*y*, −*z*+1/2; (xii) −*y*, −*x*, −*z*; (xiii) *x*−*y*, *x*−1, *z*+1/2; (xiv) −*x*+*y*, −*x*, *z*; (xv) −*y*, *x*−*y*, *z*; (xvi) *y*+1, *x*, −*z*+1/2; (xvii) −*x*+1, −*x*+*y*, −*z*+1/2; (xviii) −*x*+1, −*y*, *z*+1/2; (xix) −*x*+*y*+1, *y*, −*z*; (xx) −*y*+1, −*x*, −*z*; (xxi) *x*−*y*+1, −*y*, −*z*+1/2; (xxii) −*x*+1, −*x*+*y*+1, −*z*+1/2; (xxiii) *y*+1, *x*+1, −*z*+1/2; (xxiv) *x*−*y*+1, −*y*+1, −*z*+1/2; (xxv) *x*+1, *x*−*y*, −*z*; (xxvi) −*x*, −*x*+*y*, −*z*+1/2; (xxvii) *x*, *x*−*y*, −*z*; (xxviii) −*x*+*y*, *y*, −*z*; (xxix) *y*, *x*, −*z*+1/2; (xxx) *y*, −*x*+*y*, *z*+1/2; (xxxi) −*y*+1, −*x*+1, −*z*; (xxxii) −*x*+*y*+1, *y*+1, −*z*; (xxxiii) *x*+1, *x*−*y*+1, −*z*; (xxxiv) *x*−*y*, *x*, *z*+1/2; (xxxv) *y*+1, −*x*+*y*+1, *z*+1/2; (xxxvi) −*x*+*y*+1, −*x*, *z*; (xxxvii) *x*+1, *y*+1, *z*; (xxxviii) *y*−1, −*x*+*y*, *z*+1/2; (xxxix) −*y*, *x*−*y*−1, −*z*+1/2; (xl) −*x*+*y*, *y*−1, −*z*; (xli) *x*−*y*−1, *x*−1, −*z*; (xlii) *x*−1, *x*−*y*, −*z*; (xliii) *x*−1, *y*, −*z*+1/2; (xliv) *x*−*y*−1, −*y*, *z*; (xlv) *y*, −*x*+*y*+1, −*z*; (xlvi) −*y*, −*x*+1, *z*+1/2; (xlvii) −*x*+1, −*x*+*y*+1, *z*; (xlviii) *x*−1, *x*−*y*−1, *z*+1/2; (xlix) −*x*+1, −*y*+1, *z*+1/2; (l) −*x*, −*y*, *z*+1/2; (li) −*x*+*y*+1, *y*, *z*−1/2; (lii) −*y*, −*x*+1, *z*−1/2; (liii) *x*−*y*, −*y*+1, −*z*−1/2; (liv) *y*−1, *x*−1, −*z*−1/2; (lv) −*x*, −*y*, *z*−1/2.

(Ag4P2O6_5-140_17h_p_01)

Crystal data

$Ag_4P_2O_6$
*P*6$_3$/*mcm*
a = 5.39128 (7) Å
b = 5.39128 (7) Å
c = 6.30229 (9) Å
α = 90°
β = 90°
γ = 120°
Cu *Kα*$_{1+2}$ radiation

Data collection

2*θ*$_{min}$ = 15.006°, 2*θ*$_{max}$ = 131.997°, 2*θ*$_{step}$ = 0.007°

Refinement

R(*F*) = 0.032
16714 data points

Fractional atomic coordinates and isotropic or equivalent isotropic displacement parameters (Å^2)

	x	*y*	*z*	*U*$_{iso}$*/*U*$_{eq}$	Occ. (<1)
Ag1	0.666670	0.333330	0.000000	0.04093 (7)*	
P1	0.000000	0.000000	0.161226	0.022000*	0.500000

O1	0.266569	0.000000	0.250000	0.028000*

Atomic displacement parameters (Å²)

	U^{11}	U^{22}	U^{33}	U^{12}	U^{13}	U^{23}
Ag1	0.0483 (4)	0.0483 (4)	0.0317 (4)	0.0283 (4)	0.000000	0.000000
P1	0.012999	0.012999	0.040998	0.006300	0.000000	0.000000
O1	0.019999	0.012999	0.046998	0.006700	0.000000	0.000000